Defect Management and Crystallization Regulation for High-Efficiency Carbon-Based Printable Mesoscopic Perovskite Solar Cells via a Single Organic Small Molecule

Jinjiang Wang,[a b] Dongjie Wang,[a] Dang Xu,[a] Yang Zhang,[a] Tianhuan Huang,[a] Doudou Zhang,[a] Zheling Zhang,[a] Jian Xiong,[a] Yu Huang,[a] Jian Zhang, [*a]

[a] Engineering Research Center of Electronic Information Materials and Devices of Ministry of Education, Guangxi Key Laboratory of Information Materials, School of Materials Science and Engineering, School of Mechanical and Electrical Engineering, Guilin University of Electronic Technology, Guilin 541004, China

[b] School of Physics and Electronics Engineering, Hengyang Normal University, Hengyang 421002, China

[*] Corresponding author: Prof. Jian Zhang, E-mail: jianzhang@guet.edu.cn

Experimental section

Materials. All materials were used in their original state. Formamidinium iodide (FAI, ≥ 99.5%), cesium iodide (CsI ≥ 99.9%), methylammonium bromide (MABr, ≥ 99.5%), methylammonium iodide (MAI, ≥ 99.5%), lead (II) chloride ($PbCl_2$, ≥ 99.9%), and lead (II) iodide (PbI_2, ≥ 99.99%) were purchased from Xi'an Polymer Light Technology Corp. Dicyandiamide (DCDA, 99%) was purchased from Innochem (Beijing) Technology Co., Ltd. Dimethylsulfoxide (DMSO, ≥99.9%), N,N-Dimethylformamide (DMF, 99.8%) and Titanium di-isopropoxide bis(acetylacetonate) (75 wt % in isopropanol) were acquired from Sigma-Aldrich Co. carbon pastes, m-TiO_2 pastes, m-ZrO_2 pastes, and Fluorine-incorporated tin oxide (FTO) glass sheets were supplied by Wonder Solar Corp.

Precursor Solution Preparation. the precursor solution $Cs_{0.05}MA_{0.15}FA_{0.8}PbI_{2.96}Br_{0.04}$ was obtained as follow: 0.0042 g MABr, 0.0318 g MAI, 0.013 g CsI, 0.0112 g $PbCl_2$, 0.1376 g FAI, 0.461 g PbI_2 were dissolved in 800 μL DMF/DMSO (4:1, v/v). Lead chloride was added to modulate the crystallization of perovskite while MAI was optimized to be excessive. The 1.25 mmol/mL perovskite precursor was then stirred at 50 ℃ for 2 hours before use. 1 mL titanium di-isopropoxide bis(acetylacetonate) was diluted with 30 mL isopropanol to obtain compact-TiO_2 (c-TiO_2) precursor solution, and kept at a low temperature (2-8 °C) for future use.

Device Fabrication. The FTO conductive glass was treated by ultrasonication with a stain remover, deionized water, acetone and anhydrous ethanol for 30 min in turn. Then, a layer of c-TiO_2 about 30 nm-thick was deposited on the clean FTO by spray pyrolysis at 450℃ for 20 min. Multilayer mesoporous films of m-TiO_2(≈ 500 nm)/m-ZrO_2(≈ 2 μm)/ porous carbon electrodes (≈ 10 μm) were prepared layer by layer by screen printing technology under indoor environment (40 ± 10% RH, 30 ± 5 ℃). Each layer was annealed for 40 min at 500 ℃, 400 ℃ and 400 ℃ respectively. Subsequently, perovskite precursor solution (4.5 ~ 5.0 μL) was drop-casting on the porous carbon layer after cooled to room temperature, the device was covered with a self-made glass cover and stewing for 15min, and then annealed at 57℃ for 21 h. The drip-coating and annealing processes are carried out in an air environment (30 ± 10% RH, 25 ± 5℃).

Characterization. FTIR spectra were obtained using a SHIMADZU, IRAffinity-1S spectrometer covering the range of 400 ~ 4000 cm^{-1} for testing. The perovskite films for X-ray diffraction were deposited on glass/ITO, and were analyzed using a SmartLab LX-57B X-ray diffractometer from Rigaku Corp. UV-vis absorption spectra were captured using a Lambda 365+ UV/Vis Spectrometer of PerkinElmer Inc. The SEM

mages were taken by JEOL Ltd., JSM-7610F. The KPFM was taken by a Bruker, MultiMode 8 atomic force microscope operating in tapping mode. In-situ PL spectra were obtained by introducing an excitation laser (532 nm) into the sample through a fiber, and capturing the PL data with a detector linked to an Ocean Optics USB2000. GIWAXS tests were performed at the Xenocs Xeuss 2.0 system, the beamline utilizing a Cu X-ray source with a wavelength of 1.54189 Å, along with a Pilatus 3R 300K detector for data collection. In-situ polarizing microscope were observed by PantheraTEC POL from Motic China Group Co., Ltd. The *J-V* curves were acquired using a Keithley 2400 digital source meter under simulated AM 1.5G illumination (100 mW/cm^2) and a scanning rate of 0.01 V/s. The devices were shielded by dark, non-transparent mask with a circular aperture which provided an effective illuminated area of 0.1 cm^2. IPCE spectra were obtained by the Enlitech, QE-R with Quantum Efficiency Measurement System.

Calculation section. Electrostatic potential on the molecular surfaces was calculated by the Dmol^3 module in Materials Studio software, and the LDA parameterization method of VWN was selected as the exchange-correlation functional, and the calculation accuracy was set to medium. Electrostatic potential analysis and visualization was performed with post-processing tools of Materials Studio.

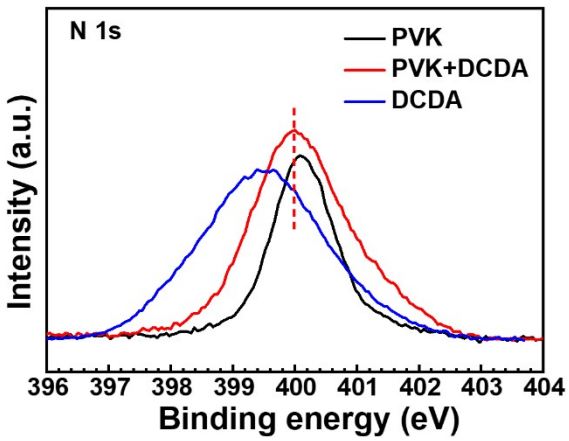

Fig. S1 High resolution XPS spectra of N 1s for the DCDA, perovskite and perovskite film modified with DCDA.

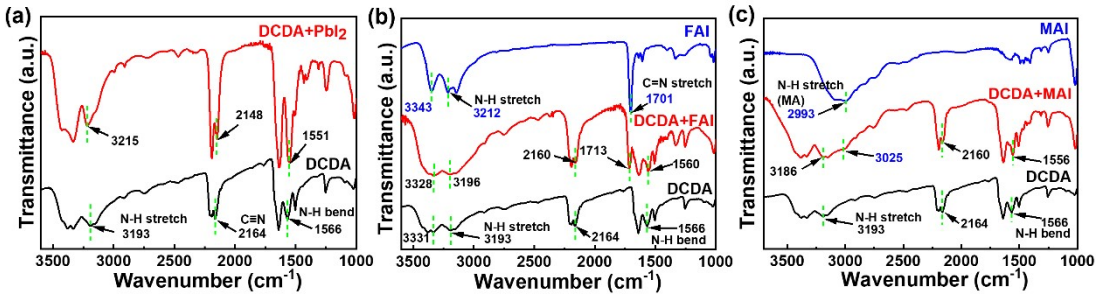

Fig. S2 a) FTIR spectra of DCDA and DCDA + PbI_2. b) FTIR spectra of DCDA, FAI and DCDA + FAI. c) FTIR spectra of DCDA, MAI and DCDA + MAI.

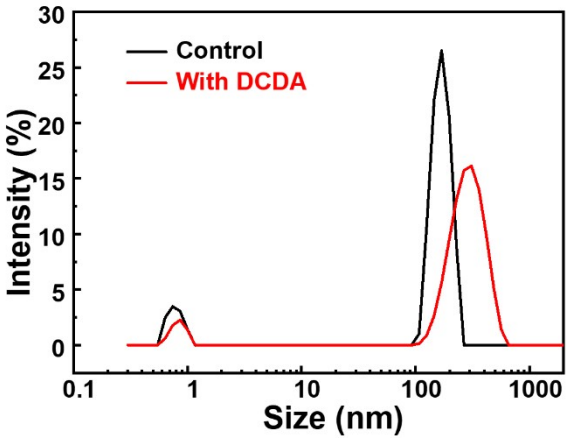

Fig. S3 DLS spectra of perovskite precursor solutions with and without DCDA.

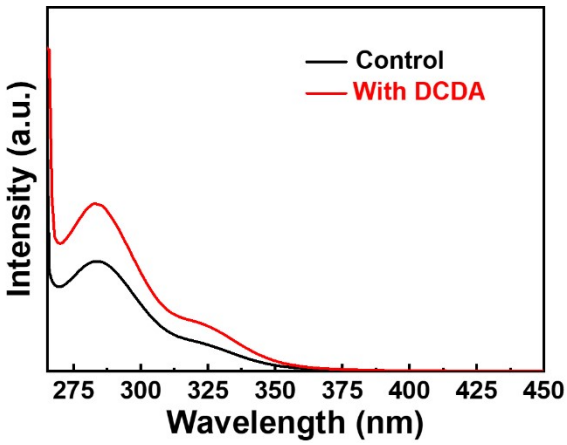

Fig. S4 UV-vis absorption spectra of perovskite precursor solutions dissolved in DMSO/DMF without and with DCDA.

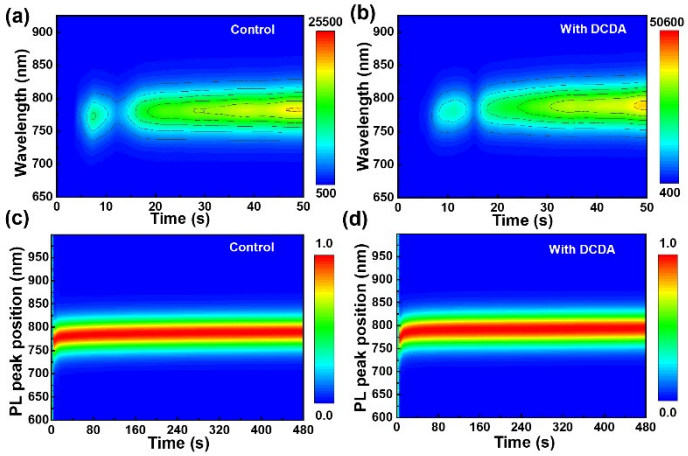

Fig. S5 (a) and (b) in-situ PL intensity evolution of the perovskite films with/without DCDA. (c) and (d) in-situ PL peak position evolution of the perovskite films with/without DCDA.

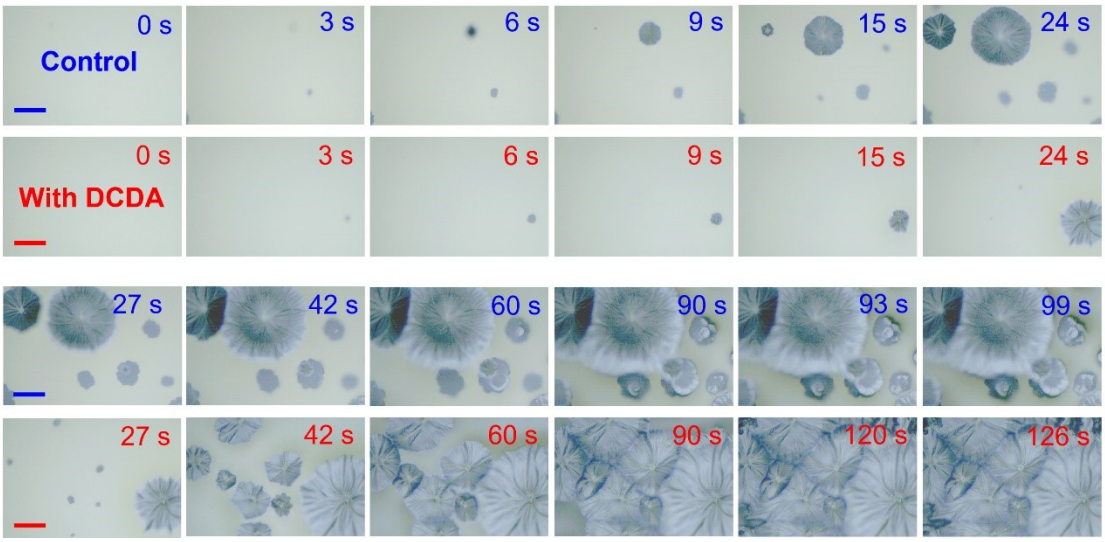

Fig. S6 The in-situ observation results of the growth process of perovskite films without and with DCDA. These images were captured using a polarizing microscope in ambient air (35 ± 10% RH and 25 ± 5℃), with a 50x objective lens and a 3-second interval between shots. The perovskite precursor solution was drop-cast onto a clean glass substrate and allowed to grow freely on a heated stage at 70 ℃. The scale of all images is 50 μ m.

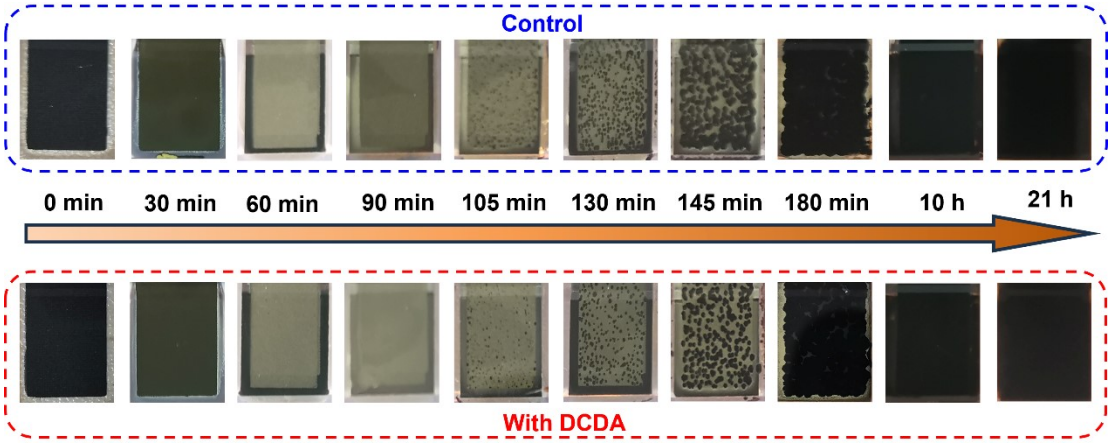

Fig. S7 The growth evolution of perovskite film without and with DCDA in the triple-mesoscopic layer at various annealing times. During the annealing process, a homemade glass cover with an inner chamber dimensions of 13 cm × 5 cm × 0.8 cm was typically employed to cover the top of device in order to prevent solvent evaporated rapidly and create an appropriate steam atmosphere conducive to the full growth of perovskite crystals. Given that the film growth was interrupted upon removal and re-place on the hot plate (maintained at a temperature of 57°C), the presented images were captured from the glass side of different devices.

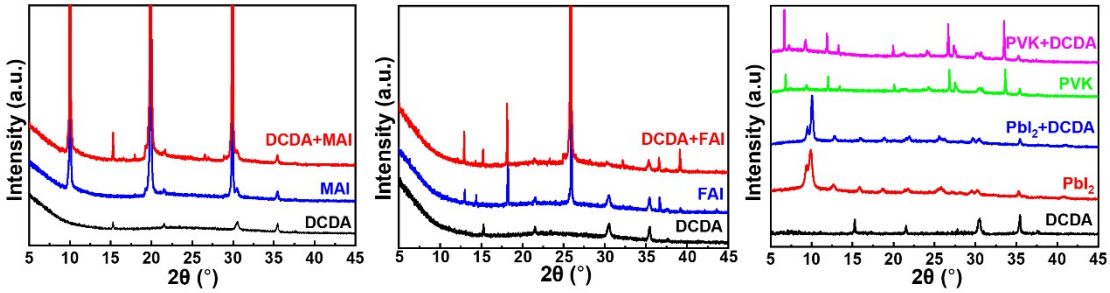

Fig. S8 XRD spectra of DCDA and perovskite components were obtained in the wet film state. All materials were dissolved either individually or together (the molar ratio of 1:1) in 1 ml of DMF:DMSO solution (4:1, v/v), followed by spin-coating onto an ITO surface at 4000 rpm and performed XRD testing after 3 min.

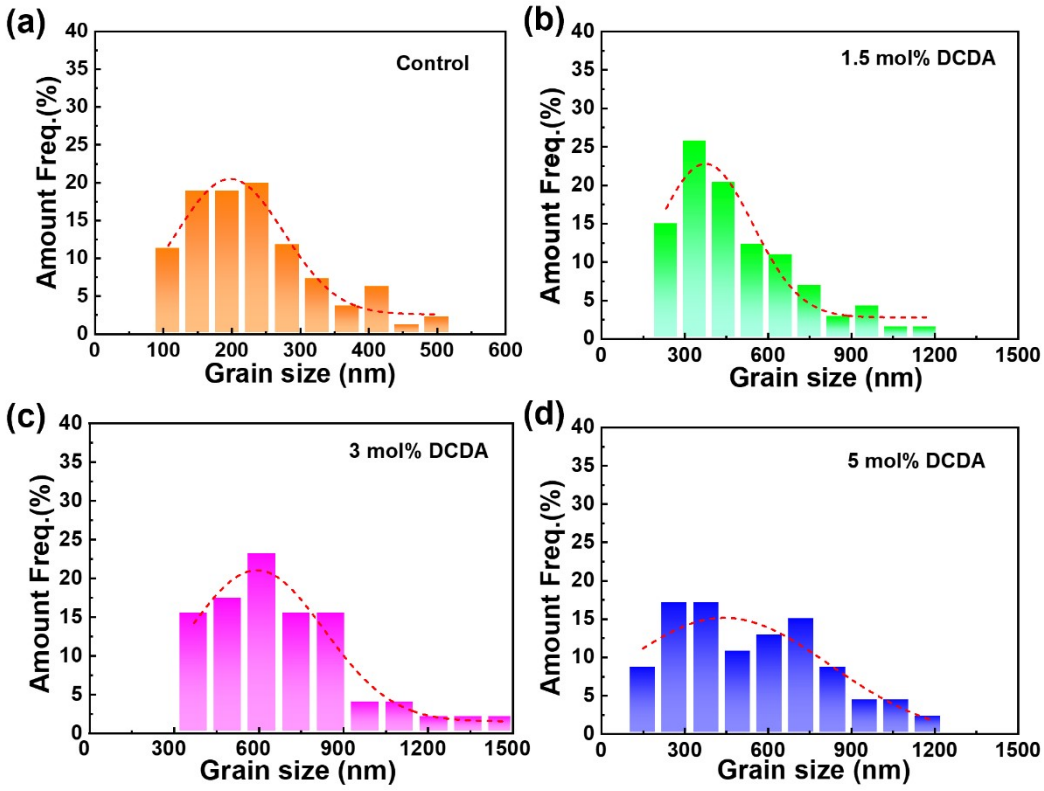

Fig. S9 a)-d) Grain size statistics for the Control, with addition of 1.5 mol%, 3 mol% and 5 mol% DCDA perovskite films.

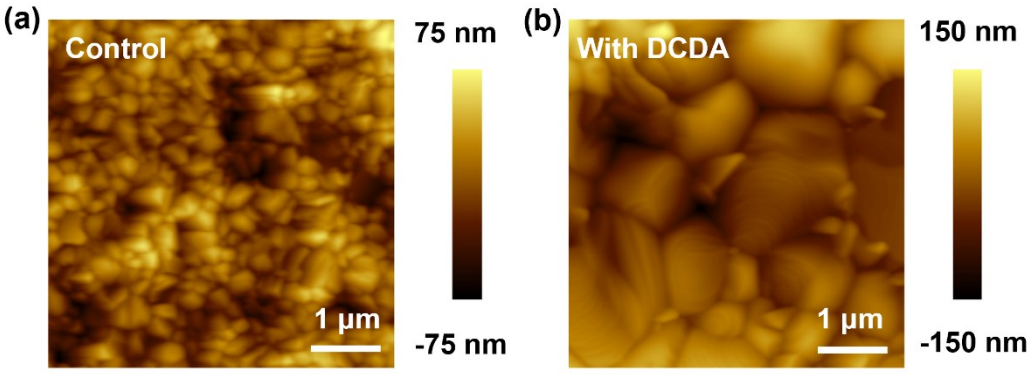

Fig. S10 AFM height images of a) the bare and b) the perovskite films treated with DCDA.

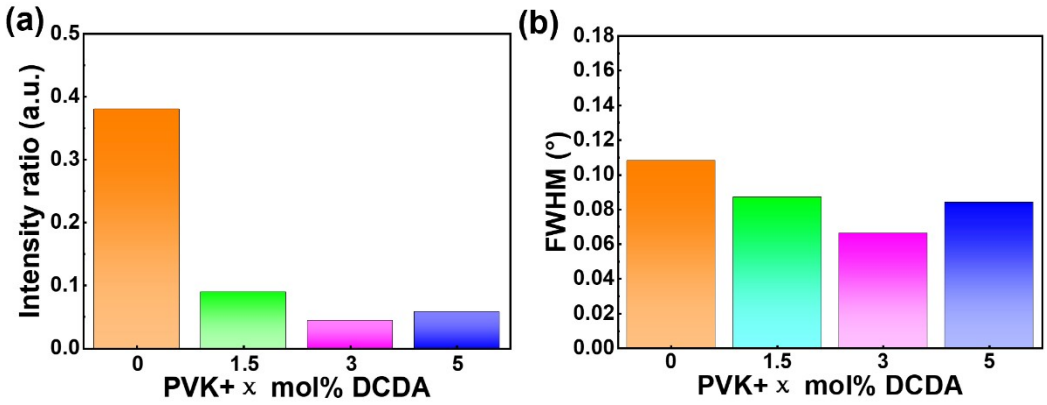

Fig. S11 The XRD diffraction intensity ratio of PbI_2 to (100) peaks of perovskites.

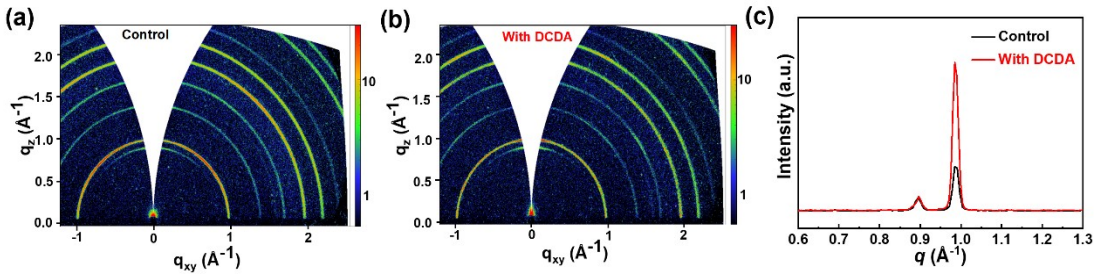

Fig. S12 2D GIWAXS patterns for a) control and b) perovskite films treated with DCDA. c) azimuthally averaged GIWAXS profiles of a) and b).

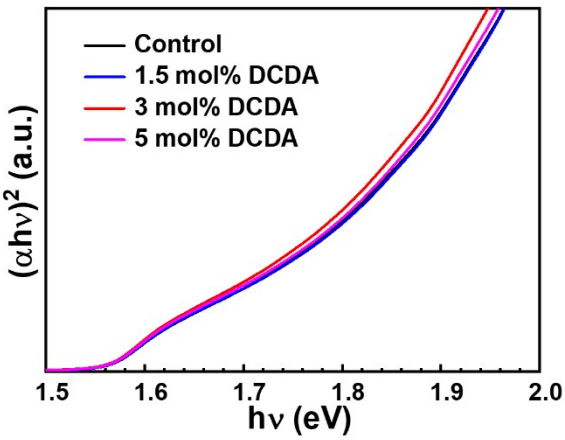

Fig. S13 Tauc plots of the solid perovskite thin films without and with different concentration DCDA.

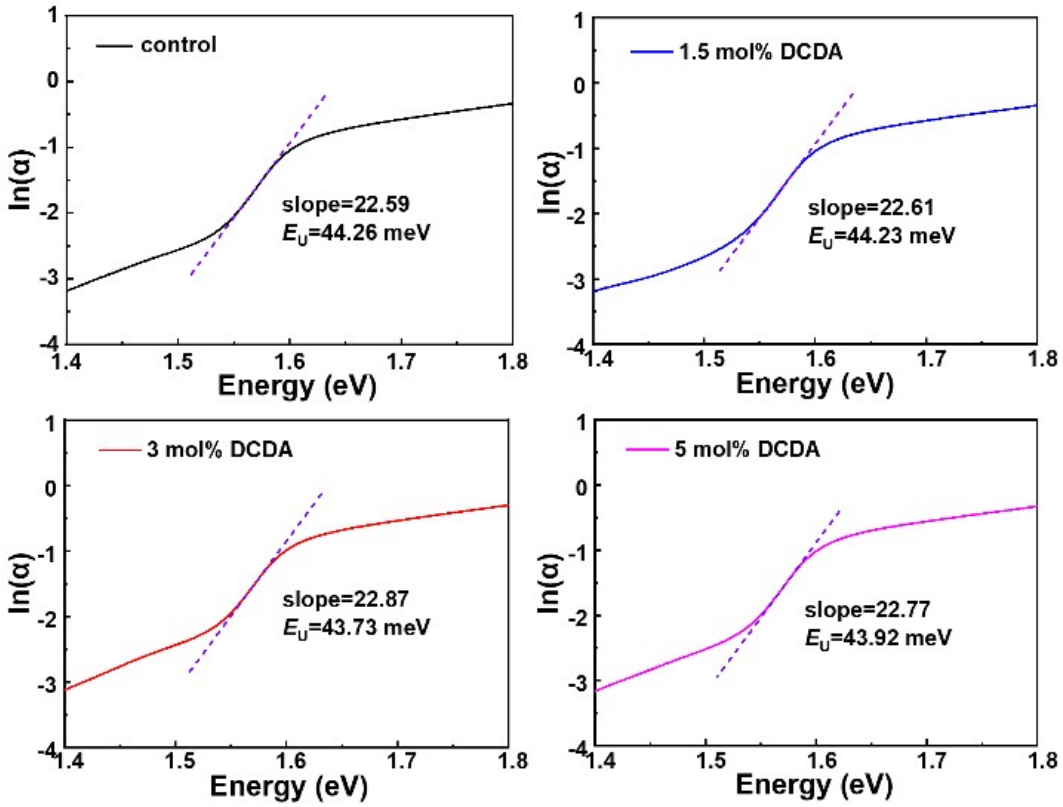

Fig. S14 Urbach energy (E_U) of perovskite films without and with variable feed ratio of DCDA.

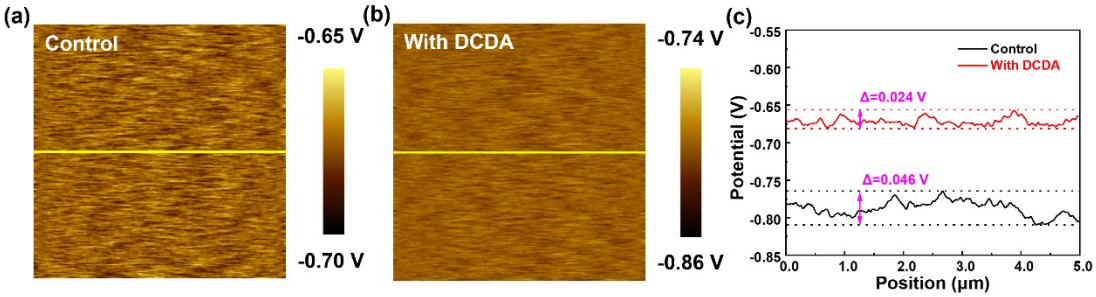

Fig. S15 a, b) Surface potential maps of the ITO/perovskite and ITO/DCDA-modified perovskite films, respectively. c) The cross-section data along the yellow line in (a) and (b).

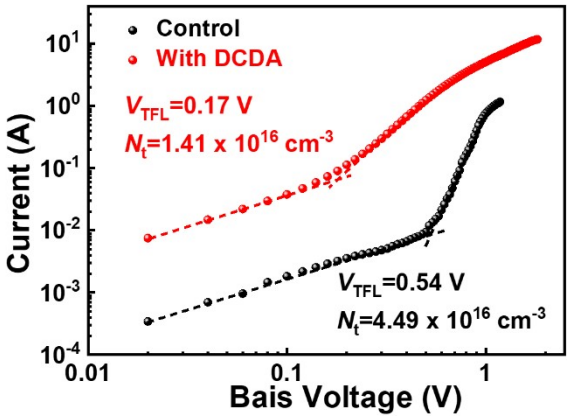

Fig. S16 SCLC characteristics of the electron-only devices.

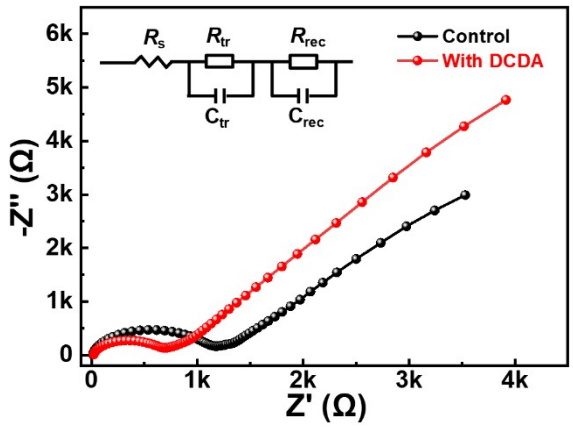

Fig. S17 EIS spectra of the control and DCDA-processed devices, and the inset is equivalent circuit model of the MPSCs in EIS.

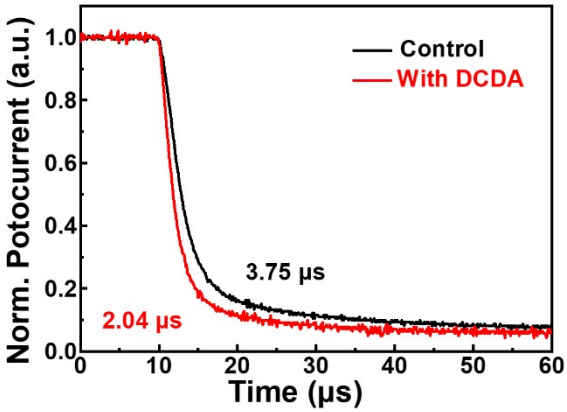

Fig. S18 Transient photocurrent decay curves of the devices with and without DCDA.

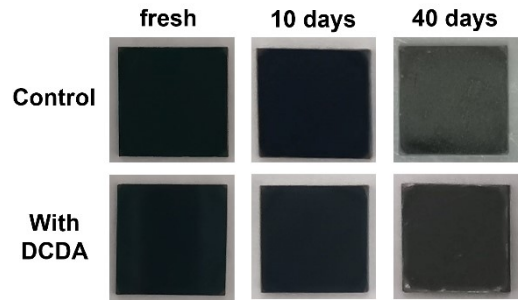

Fig. S19 Photographs of the perovskite films with and without DCDA storage in the air conditions (35 ± 10% RH, 30 ± 5℃)

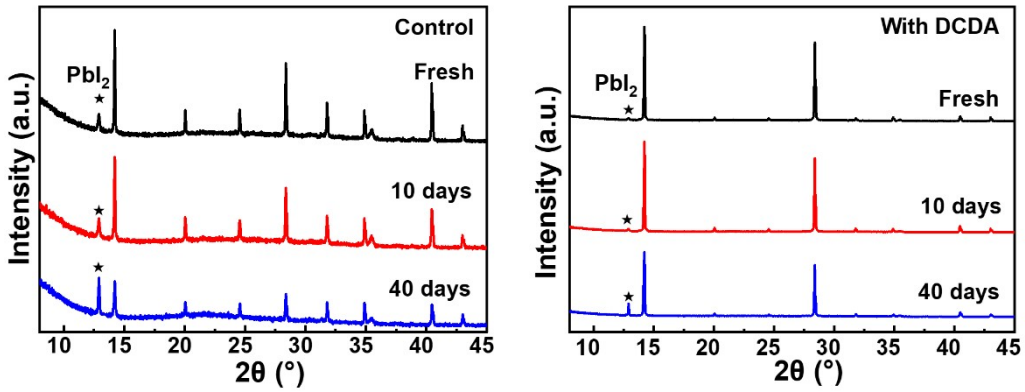

Fig. S20 XRD patterns of the perovskite films with and without DCDA storage in the air conditions (35 ± 10% RH, 30 ± 5°C)

Table S1 Optoelectronic performance parameters of the perovskite devices with different amounts of DCDA.

		V_{OC} V	J_{SC} mA cm^{-2}	FF %	PCE %
Control	average	0.981±0.021	23.29±1.20	75.06±3.60	17.15±0.48
	max	0.980	23.58	75.97	17.56
1.5 mol% DCDA	average	1.003±0.17	23.78±1.33	75.72±3.84	18.04±0.42
	max	0.999	24.28	76.08	18.45
3 mol% DCDA	average	1.009±0.020	24.41±1.09	75.96±3.65	18.75±0.42
	max	1.006	24.47	77.68	19.12
5 mol% DCDA	average	1.010±0.024	24.16±1.34	75.29±3.21	18.31±0.47
	max	1.009	24.28	76.43	18.73

All parameters are statistical data of 20 devices.

Table S2 The fitted TRPL parameters of perovskite deposited on the structure of Glass/FTO/mp-ZrO_2.

	τ_1 (ns)	τ_2 (ns)	A_1 (%)	A_2 (%)	τ_{avg} (ns)
Control	0.91	8.69	83.77	16.23	5.97
1.5 mol% DCDA	2.03	25.27	67.32	32.68	20.87
3 mol% DCDA	2.57	29.88	52.66	47.34	27.50
5 mol% DCDA	2.24	25.33	63.99	36.01	22.19

Table S3 EIS fitting parameters for PSCs without and with DCDA modifications.

Device	R_s (Ω)	R_{tr} (Ω)	R_{rec} (Ω)	C_{tr} (F)	C_{rec} (F)
Control	12.54	1121	36314	3.24×10^{-8}	8.26×10^{-5}
With DCDA	11.05	675	54859	9.84×10^{-8}	5.45×10^{-5}